10-2010

Error analysis for 3D shape measurement with projector defocusing

Ying Xu
Iowa State University

Junfei Dai
Iowa State University

Song Zhang
Iowa State University, song@iastate.edu

Error analysis for 3-D shape measurement with projector defocusing

Ying Xu[1], Junfei Dai[2] and Song Zhang[1*]

[1] Department of Mechanical Engineering, Iowa State University, Ames, IA 50011, USA.
[2] Department of Mathematics, Zhejiang University, Hangzhou, Zhejiang 310029, China.

ABSTRACT

This paper analyzes the phase error for a 3-D shape measurement system that utilizes our recently proposed projector defocusing technique. In this technique, by defocusing binary structured patterns, seemingly sinusoidal ones can be generated, and 3-D shape measurement can be performed by fringe analysis. However, there are still significant errors if the object is not within a certain depth range where the defocused fringe patterns still have binary structures. In this research, we experimentally studied a large depth range of defocused fringe patterns, from close to be binary to to be sinusoidal, and its associated phase errors are analyzed. We established a mathematical phase error function in terms of the wrapped phase and the depth z. Finally, the mathematical function is calibrated and is used to compensate for the phase error at arbitrary depth ranges within the calibration volume. Experiment will be presented to demonstrate the success of this proposed technique.

Keywords: Phase error, three dimensional; fringe analysis; defocusing.

1. INTRODUCTION

3-D shape measurement based on a digital fringe projection technique, recently emerged as a mainstream, has numerous advantages in comparison with other structured techniques including its measurement speed and accuracy.[1] Because of its simplicity and achievable high spatial resolution, there are some success using this technique for high-resolution, real-time applications.[2]

A conventional digital fringe projection projection system usually uses a commercially available digital-light-processing (DLP) projector to project computer generated sinusoidal fringe patterns. This technique could achieve reasonable speed and accuracy. However, for high-speed and high-accuracy 3-D measurement, there are three major issues to consider: (1) the nonlinearity of the projection system; (2) the precise synchronization requirement between the camera and projector; and (3) the speed bottleneck of the projector (120 Hz).[3]

To alleviate the aforementioned problems associated with a conventional fringe projection system, we recently proposed a new technique for 3-D shape measurement that utilizes the natural phenomena of projector defocusing.[4] In this technique, instead of sending sinusoidal fringe patterns to the projector, only binary structured patterns are used. The sinusoidal fringe patterns are generated by properly defocusing the projector. For this technique, because only two grayscale values (0's and 255's) are used, the nonlinear projection of the projector will not affect the measurement accuracy. In principle, the DLP projector generates grayscale value by time modulation.[5] That is, the micromirror flips ON and OFF rapidly so that the percentage of ON time represents the percentage of full grayscale value. This means that (1) to generate grayscale value 0, the micromirror is always at OFF status (0% ON); (2) to generate grayscale value 255, the micromirror is always at ON status (100% ON); and (3) to generate grayscale 128, about half time is at ON status (50% ON). Therefore, if only 0 and 255 grayscale values are used, each micromirror will stay solid without any switching, in other worlds, it is not flipping ON/OFF for each particular channel projection time. This indicates that any period of time can represent the input signal, thus the camera does not need to be precisely synchronized with the projector to capture the structured patterns.

By taking advantage of the unique features of this defocusing technology, we have successfully improved our real-time 3-D shape measurement system speed to 120 Hz.[6] Moreover, because the fringe pattern is "solid state", Gong and Zhang[7] have demonstrated that the 3-D shape measurement speed can be as fast and tens of kHz using an off-the-shelf inexpensive DLP projector (Dell M109S) with the Fourier fringe analysis method.[8] Therefore, the speed bottleneck of using a commercially available DLP projector does not exist if the defocusing technique is adopted. In addition, with advanced hardware technique, such as the DLP Discovery platform developed by the Texas Instrument, ultrafast phase shifting can be achieved, and unprecedentedly high speed 3-D shape measurement becomes feasible. Specifically, we have

*song@iastate.edu; phone (515) 294-0723; fax (515) 294-3261; www.vrac.iastate.edu/~song.

Optical Metrology and Inspection for Industrial Applications, edited by Kevin Harding, Peisen S. Huang, Toru Yoshizawa,
Proc. of SPIE Vol. 7855, 78550T · © 2010 SPIE · CCC code: 0277-786X/10/$18 · doi: 10.1117/12.870715

developed a system that we could reach 667 Hz 3-D shape measurement speed by utilizing a three-step phase-shifting approach with the DLP Discovery D4000 projection platform.[9]

However, the projector defocusing based technology is not trouble free. We found that there are significant phase errors if the object is not within a small depth range where high-quality sinusoidal fringe patterns are developed. Therefore, comparing with a conventional fringe projection technique where the fringe patterns are all sinusoidal throughout the whole range, the depth range of this defocusing technique is much smaller. To increase the depth range, the phase error needs to be dramatically reduced even when the fringe patterns are not defocused to be good sinusoidal ones. One approach is to establish the relationship between phase error and the degree of defocusing, thus an error compensation method can be adopted to compensate for the phase error if the degree of defocusing is known.

Defocusing technology has been used to remove pixel effects for a long time. But in our research we used this technique to generate sinusoidal fringe patterns for 3-D shape measurement. It should be noted that Su et al. has used the defocusing technology for 3-D shape measurement with a Ronchi grating.[10] Because the Ronchi grating is a mechanical device, it is not easy to change fringe pitches and to shift the phase. A digital fringe projection technique, on the other hand, precisely controls the phase shift and adjusts the fringe pitch easily. Therefore, it is advantageous to use such a technology for 3-D shape measurement. Unlike a grating based technique where the phase error caused by phase shift may dominant, the digital fringe projection technique does not have this type of error due to its digital fringe generation nature. Therefore, the phase errors caused by other sources needs to be considered and reduced for high-quality measurement.

In this research, we experimentally studied a large depth range of defocused fringe patterns, from close to be binary to to be sinusoidal, and its associated phase errors are analyzed. We established a mathematical phase error function in terms of the wrapped phase and the depth z. Finally, the mathematical function is calibrated and is used to compensate for the phase error at arbitrary depth ranges within the calibration volume. To quantify the phase error, an uniform flat white board is placed in front of the system and moved closer or further away from the system. For each position, the phase error is analyzed and stored into a look-up table (LUT). We found that these LUTs can be approximated as a high order polynomial function for each plane, this is called the intra-plane polynomial fitting. Moreover, we found that the phase error has the same structure in terms of wrapped phase at different depths, whilst their amplitudes varies. Therefore, the amplitude can then be approximated as another set of polynomial functions in terms of depth, z, this is called inter-plane polynomial fitting. Our experiments found that the phase error can be represented as a mathematical function in terms of the depth z and the wrapped phase value. For each measurement, if we know the depth value, the phase error can be compensated for. Experiments will be performed to verify the perfromance of this proposed phase error compensation technique.

Section 2 briefly explains the principle of the defocusing technology and the three-step phase-shifting algorithm. Section 3 analyzes the phase errors and presents the error compensation methodology. Section 4 shows some preliminary experimental results that demonstrate the success of the proposed error compensation technique, and finally, Section 5 summarizes this paper and discusses the future works.

2. PRINCIPLE

2.1 Fundamentals of defocusing technology

Our recent study showed that by properly defocusing a binary structured pattern, the quasi-sinusoidal fringe pattern can be generated; and by spatially moving the binary structured pattern, the phase shift can be introduced; and 3-D shape measurement based on a digital fringe projection and phase-shifting method can be realized using this technique .[4] To illustrate the viability of generating sinusuoidal fringe patterns by defocusing binary structured ones, we conducted an experiment. In this experiment, we used a Dell LED projector (Model: M109S) and a The Imaging Source digital USB CCD camera (Model: DMK 21BU04) to project and capture the images, respectively. The projector shines a computer generated binary structured pattern onto the an uniform flat white surface, and the camera images the scattered structured pattern into a computer. During the experiment, the camera is always in focus, the target plane holds its position, and the projector is defocused to different degrees. The degrees of defocusing are realized by adjusting the focal length of the projector. Figure 1 shows some typical fringe patterns captured by the camera during this process. It clearly shows that if the projector is defocused to different degrees, the binary structured pattern is distorted to different levels. Fig. 1(a) shows the result when both the projector and the camera are both in focus, it shows binary structures on the image. This experiment also shows that when the degree of defocusing increases, the binary structures become less and less clear, and the sinusoidal ones appear to be more and more obvious. However, when the projector is defocused too much, the

sinusoidal structures start diminishing, as indicated in Fig. 1(e). Fig. 1(f)-Fig. 1(j) plot the cross sections of the associated fringe patterns above. This experiment indicates that a seemingly sinusoidal fringe pattern can indeed be generated by properly defocusing a binary structured one.

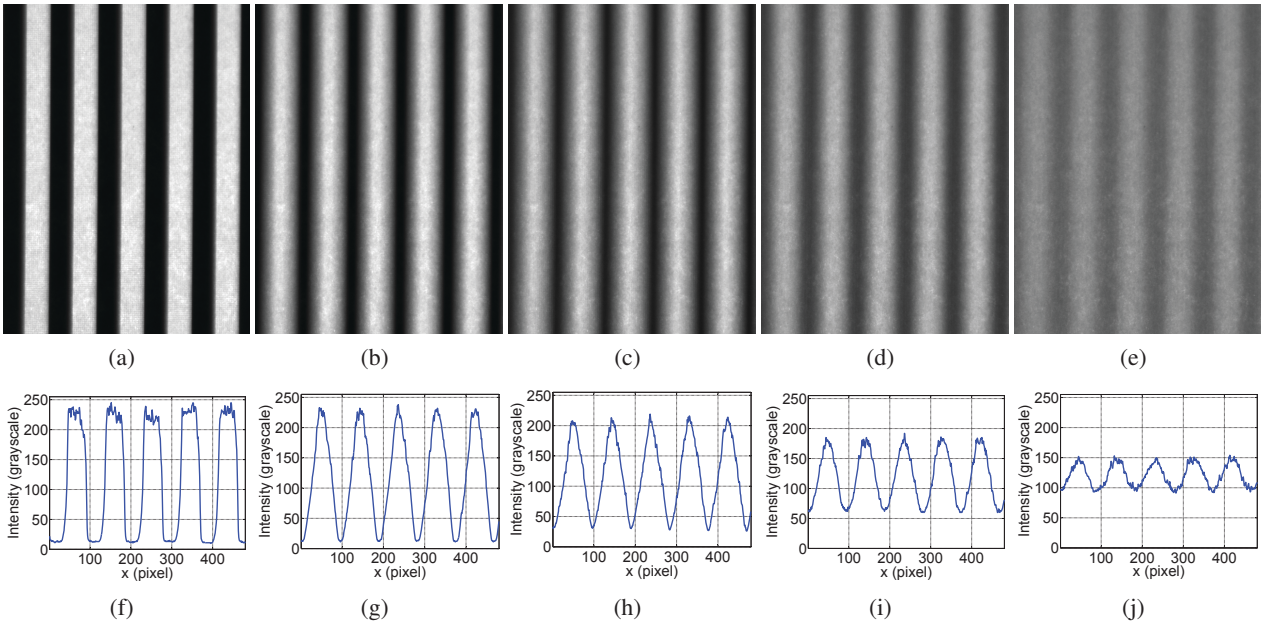

Fig. 1. Example of sinusoidal fringe generation by defocusing a binary structured patterns. (a) shows the result when the projector is in focus; (b)–(e) show the gradual results when the projector increases its defocusing degrees. (f)–(j) illustrate the 240^{th} row cross sections of the corresponding above fringe images.

2.2 Three-step phase-shifting algorithm

Phase-shifting methods have been extensively used in optical metrology because of its speed and accuracy.[11] Over the years, many phase-shifting algorithms have been developed, including three step, four step, double step, etc. Differing in the number of fringe patterns used, they share the same characteristics of (1) performing measurement point by point; (2) automatically alleviating the influence of ambient light; (3) obtaining phase value ranging from $-\pi$ to $+\pi$; and (4) achieving better accuracy by using more fringe patterns. Among these algorithms, a three-step phase-shifting algorithm is usually adopted for high speed applications because it requires the least number of fringe patterns to recover one 3-D shape. Three fringe images with a phase-shift of $2\pi/3$ can be represented as

$$I_1(x,y) = I'(x,y) + I''(x,y)\cos[\phi(x,y) - 2\pi/3], \quad (1)$$

$$I_2(x,y) = I'(x,y) + I''(x,y)\cos[\phi(x,y)], \quad (2)$$

$$I_3(x,y) = I'(x,y) + I''(x,y)\cos[\phi(x,y) + 2\pi/3]. \quad (3)$$

Where $I'(x,y)$ is the average intensity, $I''(x,y)$ the intensity modulation, $\phi(x,y)$ the phase to be solved for. Simultaneously solving Eqs. (1)–(3) will give the phase

$$\phi(x,y) = \tan^{-1}\left[\sqrt{3}(I_1 - I_3)/(2I_2 - I_1 - I_3)\right], \quad (4)$$

This equation only provides the phase value with a range of $[-\pi, +\pi)$, which is called the wrapped phase that can be unwrapped to obtain a continuous phase map, $\Phi(x,y)$, by adopting a phase unwrapping algorithm.[12] A phase unwrapping algorithm is essentially to locate the 2π discontinuous places in the wrapped map, and to remove them by adding or subtracting multiple times of 2π. In other words, the phase unwrapping is to determine integer number $k(x,y)$ for each point, so that

$$\Phi(x,y) = 2\pi \times k(x,y) + \phi(x,y). \quad (5)$$

Once the unwrapped phase is obtained and the system is calibrated, 3-D information can be recovered after system calibration.[13]

3. PHASE ERROR ANALYSIS

3.1 Experimental system setup

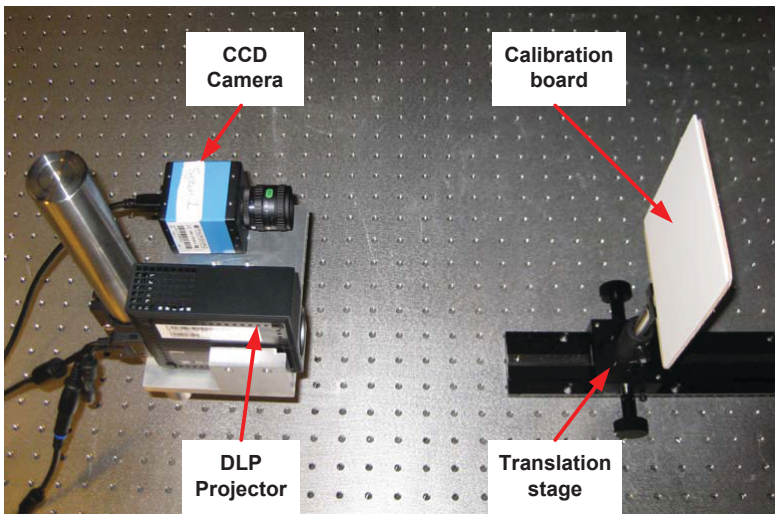

Fig. 2. Photograph of the experimental system setup.

Figure 2 shows a photograph of the experimental system setup. The 3-D shape measurement system includes a DLP projector (Model: Dell M109S) and a digital USB CCD camera (Model: The Imaging Source DMK 21BU04). The camera is attached with a 12 mm focal length Mega-pixel lens (Model: Computar M1214-MP). The resolution of the camera is 640 $\times$480, with a maximum frame rate of 60 frames/sec. The pixel size of the camera sensor is 5.6 $\times$ 5.6 μm^2. The projector has a resolution of 858 $\times$ 600 with a lens of F/2.0 and f = 16.67 mm.

A linear translation stage is used to provide the desired motion backward and forward for error analysis. In this research, we used the TECHSPEC Metric long travel linear translation stage. This stage is 250 mm long with a traveling accuracy of 0.1 mm. An uniform white flat object is mounted on top of the translation stage and travels with the srtage for this study.

3.2 Phase error determination

A three-step phase-shifting algorithm introduced in Subsection 2.2 is used the compute the phase value. The phase-shifted fringe patterns are generated by spatially moving the binary structured ones. For instance, a $2\pi/3$ phase shift can be achieved by moving the binary patterns 1/3 of its period. Our experiments found that the unwrapped phase map, $\Phi^b(x,y)$, of a uniform white board is curved instead of a planar one. This might be because the lenses distortions for the camera and/or for the projector, and the deviation of the uniform white flat surface from an ideal plane. This makes it difficult to determine the phase error only from three defocused binary patterns. To circumvent this problem, we captured three additional fringe patterns where a conventional fringe generation technique was adopted, i.e., the projector projects computer generated sinusoidal fringe patterns. It is important to note that the projector's nonlinearity is calibrated and corrected, and the exposure time we used is 1/30 second to avoid the problems associated with synchronization. From these fringe patterns, another unwrapped phase map, $\Phi^s(x,y)$, can be obtained. If the fringe pitch, number of pixels per fringe stripe is the same as that used for the binary patterns, the difference between these two phase will give the phase error induced by the binary structured patterns, that is, the phase error is calculated point by point using

$$\Delta\Phi(x,y) = \Phi^b(x,y) - \Phi^s(x,y). \tag{6}$$

Here, $\Phi^b(x,y)$ represents the unwrapped phase from the binary structured patterns, and $\Phi^s(x,y)$ represents the unwrapped phase from the sinusoidal fringe patterns.

It should be noted that this phase error is to compare against the conventional fringe projection technique, thus the Golden-standard for this technique is the result obtained from a conventional fringe projection technique. To reduce the influence of the random noise caused by $\Phi^s(x,y)$, this phase map was smoothed by a 9×9 Gaussian filter. Figure 3 shows a

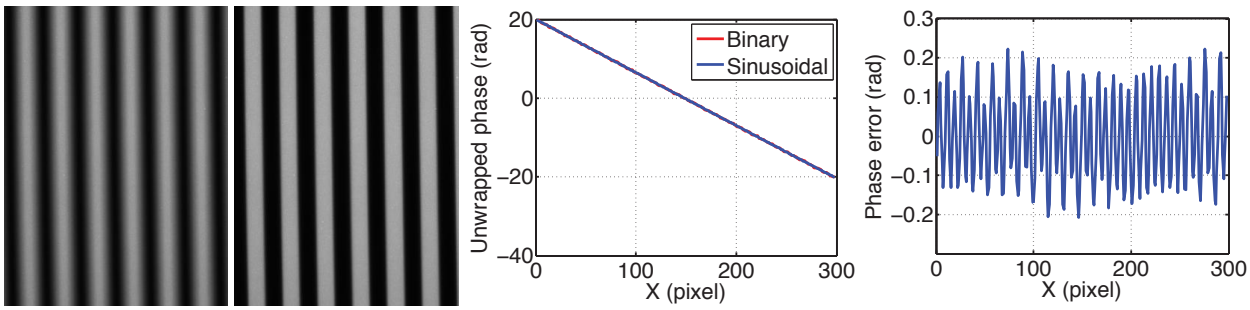

(a) (b) (c) (d)

Fig. 3. Compute the phase errors by finding the difference between the phase obtained from the sinusoidal fringe patterns, and that obtained from the defocused binary patterns. (a) One of three phase-shifted fringe patterns using the sinusoidal method; (b) One of three phase-shifted fringe patterns using the binary method; (c) Cross sections of the unwrapped phase maps; (d) Phase error.

typical result obtained by the aforementioned method. To minimize the effect of color induced problems, we only used B/W fringe patterns for both the traditional and the defocusing methods. The B/W fringe patterns are generated by equaling the grayscale values of red, green and blue channels of the projector. Fig. 3(a) shows one of the three phase-shifted sinusoidal fringe patterns, and Fig. 3(b) shows one of the defocused binary patterns. It can be seen that there are obvious binary structured in the binary fringe pattern. Figure 3(c) shows the cross sections of the unwrapped phase maps, $\Phi^s(x,y)$ and $\Phi^b(x,y)$. This figure indicates that they are indeed closely aligned together, and the difference between them will be the phase error, as shown in Fig. 3(d). The error appears to have periodical structures that could be further analyzed for error compensation. It should be noted that to reduce the sub-pixel sampling difference between the fringe patterns captured for these two methods, the phase error is offset to ensure that its average is 0.

The phase error shown in Fig. 3(d) is spatially position dependent, thus is difficult to use for further analysis. To solve this problem, we plot the phase error map against the wrapped phase ($\phi(x,y)$), as shown in Fig. 4(a). In this figure (as well as the rest figures), three cross sections of the unwrapped phase map are depicted. This clearly shows that the phase error appears to be spatially position independent in phase domain, which is desirable for future error compensation purpose. Moreover, the error map also have very obvious structures. To further verify these, we captured three additional planes and plotted the phase errors against the wrapped phase (as shown in Figures 4(b)–4(d)), they all appear to have similar structures as the first one, whist with different amplitudes. The similarity between the phase errors in different planes provide the opportunity to find a mathematical description of the phase error in terms of the wrapped phase value ($\phi(x,y)$), and the depth distance (z). Once the function is determined, the associated phase error can be compensated for. Because it is a deterministic, the phase error function can be foudn from calibration, which will be addressed next.

3.3 Phase error function calibration

To calibrate the phase error function in terms of the wrapped phase ($\phi(x,y)$) and the depth (z), we set up the system in a manner so that the projected image is focused onto a plane, and the camera is also focused at the same plane. This plane is chosen as $z = 0$, we then move the plane towards the system with an increment of $\Delta z = 5$ mm. For each plane, we recorded three phase-shifted binary patterns, and three phased-shifted sinusoidal patterns with exactly the same fringe pitch, and computed the phase error using Eq. (6). Because the phase error is depth z dependent, and the wrapped phase ϕ dependent.we can rewrite the phase error equation as

$$\Delta\Phi(x,y;z) = \Phi^b(x,y;z) - \Phi^s(x,y;z) = f(\phi;z). \tag{7}$$

To simplify the error function determination, we do the following two steps for each plane:

- *Step 1*: Create a m-element look up table (LUT) by evenly quantize the wrapped phase $[-\phi,+\phi)$ with a $2\pi/M$ rad phase interval. Within each interval, the phase error is averaged to reduce the random error for the whole image. In this research, we use a 1024 element array to store the error LUT. Figure 5(a) shows the error map for the whole image illustrated in Fig. 4(a).

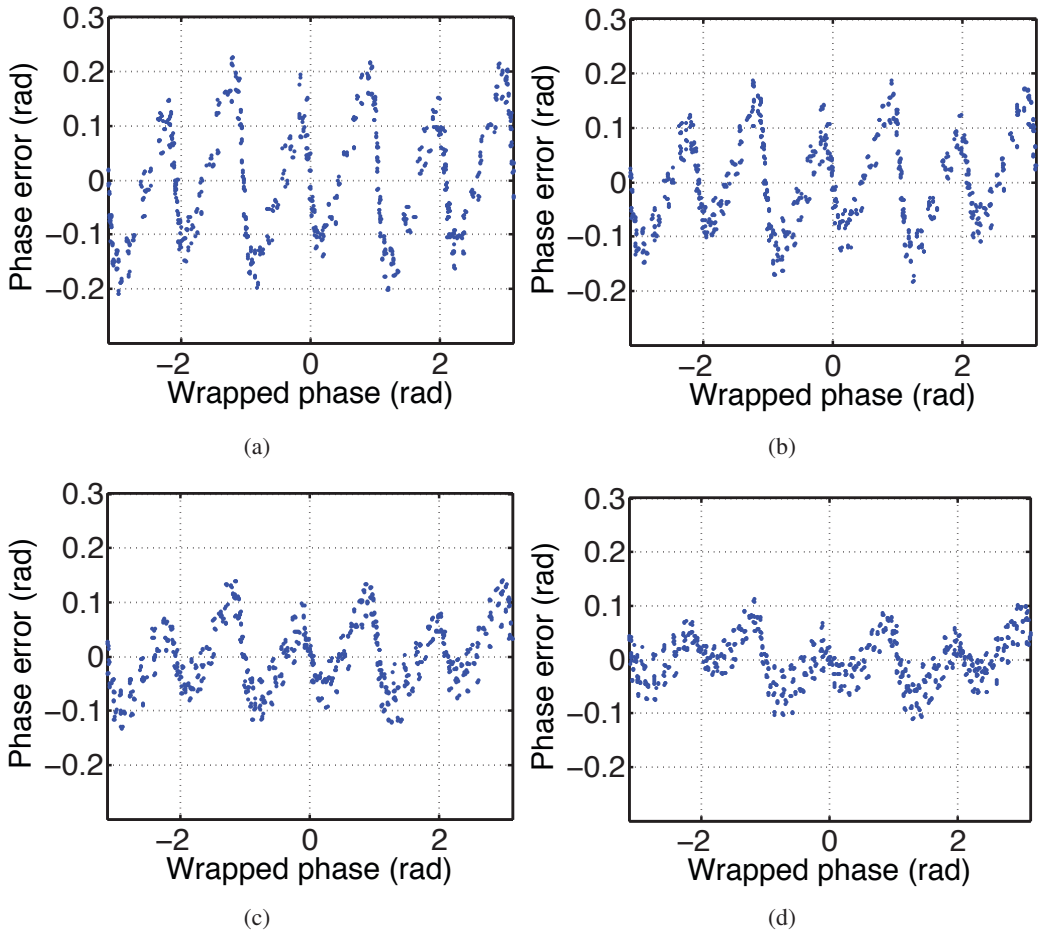

Fig. 4. Phase error maps for different depth planes. (a) Depth $z = 0$ mm; (b) Depth $z = 20$ mm; (c) Depth $z = 40$ mm; (d) Depth $z = 60$ mm.

- *Step 2*: Fitting the LUT with Nth-order polynomials $\Phi(x,y;z) = \sum_{k=0}^{N} a_k(z)\phi^k$. We found that a 40th-order polynomial is necessary in order to precisely represent the error LUT because of its complex structures. Figure 5(b) shows the overlay between the fitted polynomials and the original LUT. They seems to be aligned well with each other.

To verify the effectiveness of the LUT and the polynomial fitting, we used them to compensate for the phase errors in that particular plane. Figure 5(c) shows The residual error after the error compensation with this LUT, while Figure 5(d) shows residual error with the fitted polynomials. The phase error is reduced from originally RMS 0.108 rad, to RMS 0.028 rad with the LUT, and to RMS 0.030 rad with the fitted polynomials. It is approximately three times smaller for both methods. The polynomial fitting method performs slightly worse than the direct LUT method because it has some approximation during optimization stage. One may notice that after error compensation, not only is the magnitude of the phase error significantly reduce, but also the periodical structure of the phase error diminishes. Because the phase error after compensation appear to be random, a standard random noise reduction method (e.g., a Gaussian filtering) can be adopted to further reduce their influence. This experiment demonstrated the effectiveness of phase error reduction by both the LUT-based method and the polynomial-based approach.

This prior error fitting approach introduced is called intra-plane error fitting. Figure 4 also shows the phase error is depth distance z dependent. Once the error functions for different depths are determined, the polynomial coefficients can be further fitted with polynomials in terms of distance z. These polynomials are called inter-plane error fitting. Finally, the

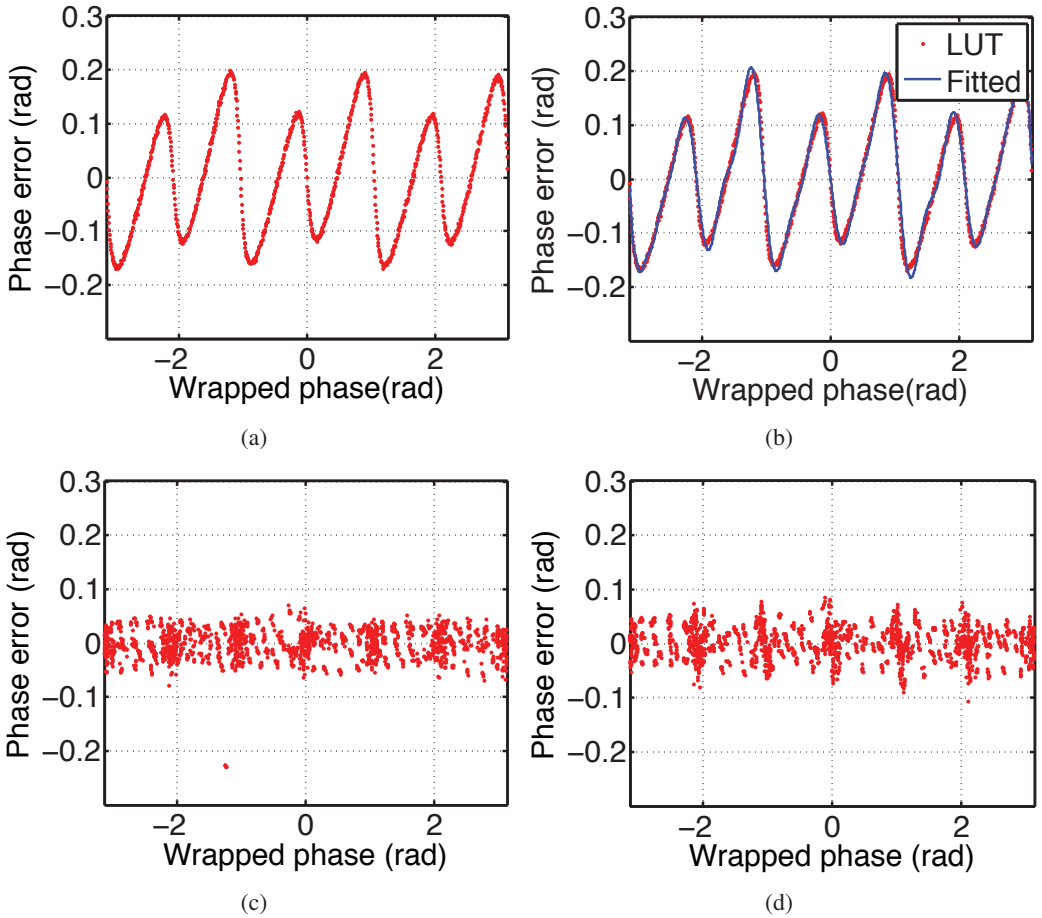

Fig. 5. Phase error compensation using the LUT and the polynomial fitting. (a) The LUT in terms of wrapped phase value; (b) Polynomial fitted curve; (c) The residual error after compensation using the LUT shown in (a) (RMS: 0.028 rad) ; (d) The residual error after compensation using the fitted polynomials (RMS: 0.030 rad).

error function can be written in the following equation,

$$\Phi(x,y;z) = \sum_{k=0}^{N} \left(\sum_{l=0}^{M} c_{k,l} z^l \right) \phi^k. \tag{8}$$

Here, $c_{k,l}$ are constants. In this research, we found that at least N = 40^{st}-order polynomials are needed for intra-plane fitting, and at least M = 4^{th}-order polynomials are needed for inter-plane fitting (coefficient fittings).

To calibrate the phase error function, we measured 34 planes and with an distance interval of $\delta z = 5$ mm. Among these planes, 15 of them are used for the polynomial function calibration, and the rest planes are used for validation purpose. The phase errors for each of these calibration planes are calculated and fitted with intra-plane polynomials, and the coefficients of these polynomials are further fitted with inter-plane polynomials. Once $c_{k,l}$ is determined, they can be used for error compensation.

4. EXPERIMENTAL RESULTS

To verify the performance of the error functions obtained above. We tried to compensate for the phase error of an plane that was not used for the polynomial function calibration ($z = 5$ mm). Figure 6(a) plots the original error against the wrapped phase. The RMS error is found to be 0.108 rad. To find out the correctness of calibrated polynomials to represent the phase error of this plane, we calculated the LUT directly from the phase error from this particular plane, computed the phase

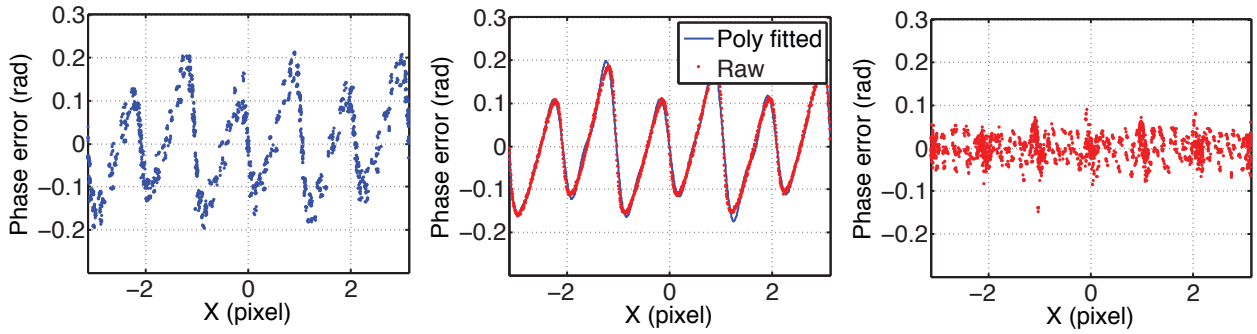

(a) (b) (c)

Fig. 6. Error reduction by polynomial fitting. (a) The original error (RMS: 0.108 rad); (b) The original LUT and the LUT with polynomial fittings; (c) Error after applying the error compensation approach introduced in this paper (RMS: 0.030 rad).

error using the calibrated polynomial function Eq. (8) by plugging in depth value $z = 5mm$. Figure 6(b) shows the result. This experiment indicates that the calibrated polynomial function well represents the error function of this plane, thus can be used to compensate for the error of this plane. Figure 6(c) shows the result after compensation. The RMS value is dramatically reduced from 0.108 rad to 0.030 rad, and the error map appears to random, similar to those plane that were used to estimate the error function. This experiment verified the success of the proposed error compensation approach to compensate for the phase error in an arbitrary plane.

5. SUMMARY

This paper has presented a method to compensate for the phase error caused by the binary structured patterns. The preliminary experimental results showed that the error function can be approximated as a polynomial function in terms of wrapped phase ($\phi(x,y)$) and the depth z, and this phase error function can be determined by calibration. Once the error function is calibrated, it can be used to compensate for the phase error caused by different level of defocusing, which is represented as the difference depth z. Experiments had been conducted and verified that this approach could reduce the phase error approximately 3 times smaller, and could effectively alleviate the periodical structure of the original phase errors. However, we used 40^{th}-order polynomials to represent the intra-plane phase error function, which is very time consuming for calculations and may result in inaccuracy with for the calculation. In the future, we plan to find a better and more efficient methodology to represent and compensate for the phase error induced by the projector defocusing.

REFERENCES

[1] Gorthi, S. and Rastogi, P., "Fringe projection techniques: Whither we are?," *Opt. Laser. Eng.* **48**, pp. 133–140, 2010.

[2] Zhang, S., "Recent progresses on real-time 3-d shape measurement using digital fringe projection techniques," *Opt. Laser Eng.* **48**(2), pp. 149–158, 2010.

[3] Lei, S. and Zhang, S., "Digital sinusoidal fringe generation: defocusing binary patterns vs focusing sinusoidal patterns," *Opt. Laser Eng.* **48**(5), pp. 561–569, 2010.

[4] Lei, S. and Zhang, S., "Flexible 3-d shape measurement using projector defocusing," *Opt. Lett.* **34**(20), pp. 3080–3082, 2009.

[5] Hornbeck, L. J., "Digital light processing for high-brightness, high-resolution applications," in *Proc. SPIE*, **3013**, pp. 27–40, 1997.

[6] Gong, Y. and Zhang, S., "Improve 4-d shape measurement speed by using projector defocusing," in *Proc. SPIE*, *SPIE Optics & Photonics* **7790**, p. 77901A, (San Diego, CA), 2010.

[7] Gong, Y. and Zhang, S., "Ultrafast 3-d shape measurement with an off-the-shelf dlp projector," *Opt. Express* **18**(19), pp. 19743–19754, 2010.

[8] Takeda, M. and Mutoh, K., "Fourier transform profilometry for the automatic measurement of 3-d object shape," *Appl. Opt.* **22**, pp. 3977–3982, 1983.

[9] Zhang, S., Weide, D., and Olvier, J., "Superfast phase-shifting method for 3-d shape measurement," *Opt. Express* **18**(9), pp. 9684–9689, 2010. (Selected for July 6, 2010 issue of The *Virtual Journal for Biomedical Optics*).

[10] Su, X. Y., Zhou, W. S., Von Bally, G., and Vukicevic, D., "Automated phase-measuring profilometry using defocused projection of a ronchi grating," *Opt. Commun.* **94**, pp. 561–573, 1992.
[11] Malacara, D., ed., *Optical shop testing*, John Wiley and Sons, New York, 3rd ed., 2007.
[12] Ghiglia, D. C. and Pritt, M. D., *Two-dimensional phase unwrapping: Theory, algorithms, and software*, John Wiley and Sons, Inc, 1998.
[13] Zhang, S. and Huang, P. S., "Novel method for structured light system calibration," *Opt. Eng.* **45**(8), p. 083601, 2006.